THE JOURNAL OF PHYSICAL CHEMISTRY LETTERS
A JOURNAL OF THE AMERICAN CHEMICAL SOCIETY

pubs.acs.org/JPCL Letter

Enhancing Defect Tolerance with Ligands at the Surface of Lead Halide Perovskites

Tyler J. Smart, Hiroyuki Takenaka, Tuan Anh Pham, Liang Z. Tan, Jin Z. Zhang,* Tadashi Ogitsu,* and Yuan Ping*

Cite This: *J. Phys. Chem. Lett.* 2021, 12, 6299–6304 Read Online

ACCESS | Metrics & More | Article Recommendations | Supporting Information

ABSTRACT: High defect tolerance has been considered a primary reason for the long charge carrier lifetime and high photoluminescence quantum yield in bulk lead halide perovskites (LHPs). On the other hand, surface defects play a critical role in determining charge carrier dynamics and optical properties, especially for LHP nanocrystals and quantum dots. Understanding the nature of surface defects and developing strategy for their effective passivation are thus of strong interest. Focusing on a prototypical LHP, $CsPbBr_3$, our work uses first-principles calculations to reveal that interstitial sites and antisites can have lower formation energies when they form at the surface while simultaneously creating deep trap states within the bandgap. Meanwhile, the formation of halide vacancies is energetically less favorable. On the basis of a new surface defect model, we demonstrate the explicit role of molecular ligands in passivating these defects, which eliminate trap states in favor of shallow states and enhance photoluminescence.

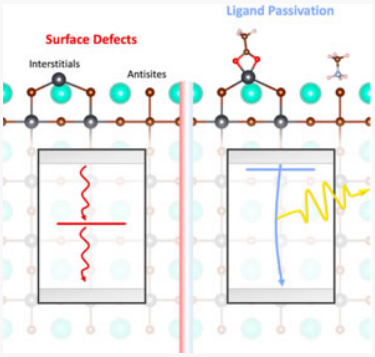

The intrigue of lead halide perovskites (LHP) is immense, owing in part to their remarkable solar conversion efficiency (~25%).[1,2] In particular, unique optoelectronic properties, including large absorption coefficient and low effective mass and long carrier diffusion length as well as long electron–hole recombination time, have prompted LHPs to garner heightened attention.[2,3] Meanwhile, their formation as nanocrystals (NCs), quantum dots (QDs), magic-sized clusters (MSCs), and two-dimensional lattices are particularly interesting to researchers due to their bandgap tunability, large spin–orbit couplings, and high photoluminescence quantum yield (PLQY) for various optoelectronic and spintronic applications.[4−11]

Particularly important to LHP's optoelectronic properties and stability is the role of defects, especially those at surfaces.[12−14] Bulk LHP is known for exhibiting "high defect tolerance," as intrinsic defects that are likely to form are simultaneously shallow.[15] However, the PLQYs of NCs are usually much lower than unity as a result of trap states from a high density of surface defects due to their much larger surface-to-volume ratio than bulk. Furthermore, experimental studies suggest that surface defects associated with deep trap states are responsible for reducing the PLQY of LHP.[16] To date, halide vacancies are believed to have a relatively low formation energy in bulk LHP[15] and result in bandgap states below the conduction band edge that can trap photoexcited electrons.[17] However, the identification of surface defects remains the subject of debate, as defect formation energy and defect levels are drastically different in bulk compared to the surface.[18,19] Furthermore, if halide vacancies were solely responsible for diminishing PLQY, it would contradict experimental studies that suggest that trap states are formed even under halide-rich conditions.[20] On the other hand, passivation,[21−25] in particular by molecular ligands, has been shown to be an effective strategy to remove defect states in the bandgap and increase stability.[6,7,16] Given the ternary nature of the LHP, one may anticipate multiple defects on the surface, which would necessitate a combination of ligands for passivation.[13]

Previous theoretical studies on surface defects of LHPs have some inconsistent findings, and most importantly, the role of ligand passivation on defect properties remains elusive. For example, charge surface defect formation energy calculations have been performed for $MAPbI_3$, but with varying results as some suggest that halide vacancies and interstitials act as carrier traps[19] while others found that lead interstitial atoms and antisites are sources of carrier traps.[26] Meanwhile previous studies have shown that, in $CsPbBr_3$ nanocrystals, the formation energy of vacancies in general is high compared to those of interstitials and antisites,[18] while others have provided some evidence that halide vacancies are responsible for diminishing PLQY observed in experiments.[17] Furthermore, lower surface formation energy has been demonstrated for ligand-terminated $CsPbBr_3$;[27] however, the explicit role and

Received: April 16, 2021
Accepted: June 29, 2021
Published: July 6, 2021

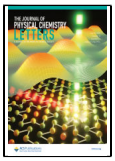

https://doi.org/10.1021/acs.jpclett.1c01243
J. Phys. Chem. Lett. 2021, 12, 6299–6304

interaction of molecular ligands with various surface defects, which may act as carrier traps, is in need of further investigation.

In this letter, using first-principles calculations, we investigate the structural and energetic properties of surface defects and associated molecular ligand passivation for a prototypical LHP, $CsPbBr_3$. Calculations of the charged surface defect formation energies reveal that both the Br_{Pb} antisite and Pb_i interstitial site have simultaneous low formation energies and result in deep bandgap trap states. The predicted breakdown of defect tolerance at the surface by first-principles calculations is interpreted in terms of molecular orbital theory. Furthermore, we demonstrate strategic passivation of these defects by eliminating deep trap states in favor of shallow ones via a charge transfer between molecular ligands and surface defects. The work provides an in-depth theoretical description of how ligands at the surface of perovskites enhance defect tolerance that can potentially improve optical properties such as photoluminescence quantum yield of LHP.

To determine the relationship between surface defects and bandgap trap states of $CsPbBr_3$, we evaluate the formation energy of several surface defect sites via first-principles calculations. Possible intrinsic defects investigated include vacancies (V_{Cs}, V_{Pb}, V_{Br}), interstitials (Cs_i, Pb_i, Br_i), and antisites (Cs_{Pb}, Cs_{Br}, Pb_{Cs}, Pb_{Br}, Br_{Cs}, Br_{Pb}) at the surface of $CsPbBr_3$, as shown in Figure 1, where A_B denotes substituting

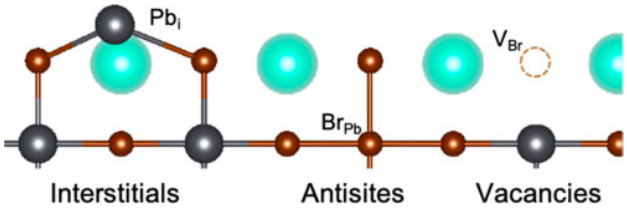

Figure 1. Schematic atomic structure of intrinsic defects considered in this work: interstitials, antisites, and vacancies. Atomic colors are as follows: Cs = cyan, Pb = gray, and Br = brown.

atom B with atom A. Density functional theory (DFT) calculations were performed using the open-source plane-wave code QuantumESPRESSO.[28] To avoid net dipoles, a symmetric slab model was constructed from the cubic phase (α-phase) of $CsPbBr_3$ by cutting the (100) direction with a Cs−Br termination with converged lateral size and vacuum length. This phase/termination is chosen based on the preference for cubic crystallinity in nanocrystals[29] and lower surface energy for this termination.[18,27] Initial atomic relaxations and screening of all intrinsic defect formation energies were carried out with the semilocal PBE functional and ultrasoft pseudopotentials[30] to reduce their computational expense. Final single-point calculations used the Heyd−Scuseria−Ernzerhof (HSE) hybrid functional including spin−orbit coupling (SOC) (α = 0.43), which reproduces electronic bandgap of $CsPbBr_3$[15] and is necessary for accurately computing band edges for defect formation energy.[31] HSE calculations are performed with norm-conserving pseudopotentials.[32] For systems with charged defects, we include a charged-defect correction to account for spurious charge interactions.[33] Additional computational details are provided in the Supporting Information.

First, the chemical potential energy of atomic Cs, Pb, and Br (denoted $\Delta\mu_{Cs}$, $\Delta\mu_{Pb}$, and $\Delta\mu_{Br}$) were obtained by evaluating the thermodynamic equilibrium growth conditions of $CsPbBr_3$ (details in the Supporting Information). The resulting phase diagram of bulk $CsPbBr_3$ is shown in Figure 2a and reveals a narrow range of chemical potential energy values wherein $CsPbBr_3$ is stable (gold region), in agreement with previous studies.[15,34] This region naturally defines a Br-rich/Pb-poor limit (denoted R_1) and a Br-poor/Pb-rich limit (denoted R_3), as well as an intermediate position (denoted R_2).

For each of these situations, the charged surface defect formation energy is calculated and shown in Figure 2b, with details given in the Supporting Information. For simplicity, only the defects that are most stable and likely to form, based on their low formation energy, are shown and labeled within the figure (full results can be found in Figure S1). Specifically, the antisites Br_{Pb} and Cs_{Pb}, in addition to each interstitial Pb_i, Br_i, and Cs_i, are found to be most likely to form at the surface of $CsPbBr_3$. In contrast, we found antisites and interstitials defects are energetically less favorable in the bulk (see Table S1). This is consistent with earlier studies[15] and highlights important differences between surface and bulk defects. For example, Pb_i in bulk shares a site with another Pb atom, forming a Pb−Pb dimer that breaks several Pb−Br bonds in the bulk material, yielding relatively higher formation energies, whereas at the surface Pb forms new bonds with dangling Br as shown in Figure 3, parts a and b (further details in the Supporting Information). In the case of Br_{Pb} (Figure 3c,d), the substituted Br creates a tribromide anion (Br_3^-) at the surface with bond lengths (2.52 and 2.58 Å) similar to those found in molecular complexes (2.44−2.67 Å),[35] whereas in bulk they are constrained to be much longer (3.06 Å), indicative of weak binding of the substituted Br. On the other hand, the formation of halide vacancies at surface and in bulk are chemically similar and there is only a slight decrease in energy by forming at the surface (Table S1 and related discussion).

Besides demonstrating stability, the charged defect formation energy also provides defect charge transition levels (CTLs) that reveal whether the defects result in deep trap states. CTLs for such defects are shown in Figure 2c, namely Pb_i, Cs_{Br}, Br_{Pb}, Pb_{Br}, and Pb_{Cs}, all result in states far from the band edges (e.g., greater than 0.5 eV, shown in Figure S2). Similar to what we find in bulk (see Figure S3 and related discussion), at the surface the formation of Br−Br or Pb−Pb bonds creates deep trap states from antibonding and bonding interactions in the valence and conduction bands, respectively (Figure 3e). For example, this is observed in the case of Br_{Pb}, where Br−Br bonds create antibonding states in the gap (for bulk and surface formation). In addition, at the surface, defects can also create deep trap states by exposing dangling bonds, such as the case of Pb_i. Ultimately, we find an important contrast in the defect tolerance (e.g., the ability to resist forming defects which create deep trap states) between the bulk and the surface. More specifically, bulk LHPs exhibit strong defect tolerance due to the electronic character of the valence and conduction band, which does not originate from bonding/antibonding splitting.[36] Hence, defects in bulk with low formation energy do not lead to deep trap states.[15] However, while the electronic character of the surface remains the same as that of bulk, drastic lowering in formation energy coupled with existence of deep trap states (e.g., in the case of Pb_i and Br_{Pb}, see Figure 2d) suggests that defect tolerance breaks down at the LHP surface.

https://doi.org/10.1021/acs.jpclett.1c01243
J. Phys. Chem. Lett. 2021, 12, 6299−6304

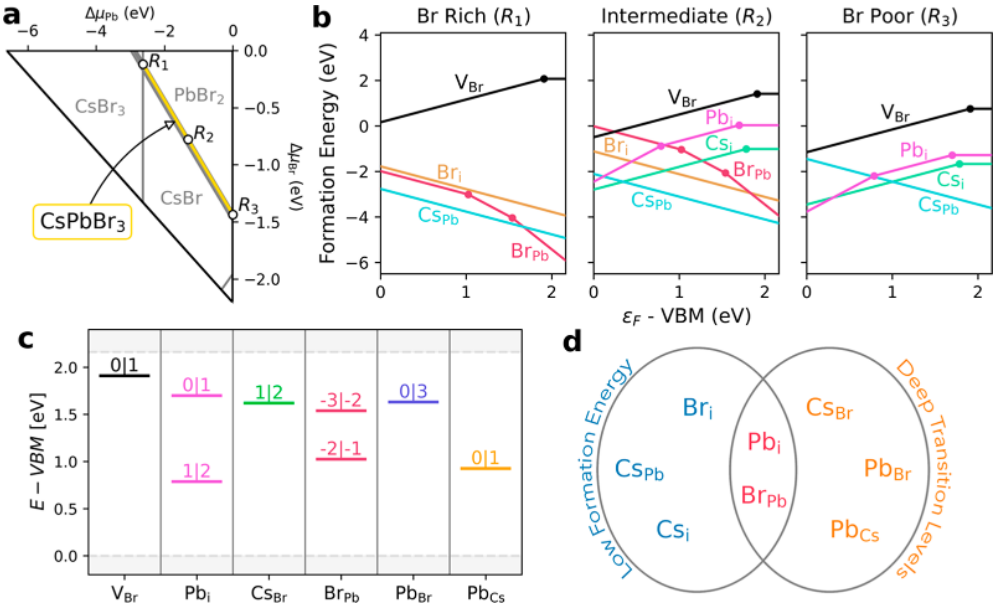

Figure 2. Charged defect formation energy at the $CsPbBr_3$ surface. (a) Phase diagram of bulk $CsPbBr_3$ with stable region in gold color. (b) Surface defect formation energy of defects at Br-rich, intermediate, and Br-poor condition as defined by R_i in part a. (c) Charge transition levels (CTLs) of defects at $CsPbBr_3$ surface, where qlq' denotes a transition from charge state q' to q. (d) Venn diagram demonstrating surface defects that simultaneously possess low formation energy and deep trap states.

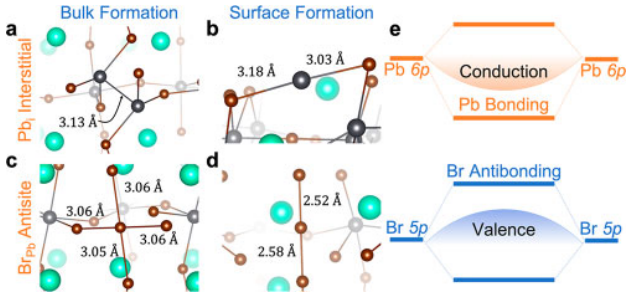

Figure 3. Rationalizing formation of deep defects at the bulk and surface of $CsPbBr_3$. Formation of (a) Pb_i in bulk yields a shared site with a Pb–Pb dimer and a Pb–Pb distance of 3.13 Å. (b) Pb_i at the surface, which coordinates with two surface Br atoms, has bond lengths similar to the pristine bulk Br–Pb bond (~3.0 Å). (c) Br_{Pb} in the bulk weakly binds to neighboring Br with bond lengths (~3.06 Å). (d) Br_{Pb} at the surface forms a Br trimer with bond lengths (2.52 and 2.58 Å). (e) Deep transition levels in $CsPbBr_3$ can occur from Br–Br antibonding (c and d), Pb–Pb bonding (a), or a Pb dangling bond (b).

Intriguingly, these two defects (Br_{Pb} and Pb_i) experience low formation energy at opposite limits of chemical condition, specifically they have low formation energies in Br-rich and Br-poor conditions, respectively (see Figure 2a). This is consistent with experimental observations that both Br-rich and Br-poor environments can experience reduced PLQY of LHP nanocyrstals.[20] Meanwhile, as mentioned above, halide vacancies are commonly reported to be responsible for creating trap states. In contrast, we find that V_{Br} is shallow and with relatively higher surface formation energy (black line in Figure 2b). Our observation that V_{Br} is not a likely source of creating trap states at the surface is consistent with some previous studies,[18,19,26] even though not broadly recognized.[36] As a result, we suggest that Pb_i and Br_{Pb} should play a more significant role at the surface than V_{Br} in the optical properties such as PLQY. We will consider V_{Br} along with the proposed Pb_i and Br_{Pb} defects in the rest of the letter as we address the issue of ligand passivation of surface defects.

Ligand passivation is an effective strategy to stabilize LHPs by addressing surface defects. Namely, molecules such as the oleate (anionic) and oleylammonium (cationic) ligands have provided successful passivation of LHP surfaces.[6,7] In this work, the rationale for defect passivation is provided in Table 1. For *n*-type defects (V_{Br}, Pb_i) we find acetate (CH_3COO^-) strongly binds to the surface at the impurity site, whereas methylammonium ($CH_3NH_3^+$) strongly binds to *p*-type defects (Br_{Pb}). Binding energies, as well as charged defect formation energies with ligands are computed using methods similar to those used in ref 37, as detailed in the Supporting Information. Since the formation of *n*-type/*p*-type defects is dependent on chemical condition as discussed above, the strategy of ligand passivation also needs to adapt for optimal effect.[13] The negative binding energies (BE) in Table 1 indicate that these ligands are appropriate for attaching to such defects, consistent with experimental studies[6,7] and previously reported theoretical results.[21] The local structure of the ligand-terminated defects is shown in Figure 4. We find that both V_{Br} and Pb_i exhibit dangling Pb bonds at the surface that can form a strong bond with both O's of the acetate, consistent with recent experimental observation of passivating undercoordi-

Table 1. Strategy of Defect Passivation by Ligands[a]

defect	type	ligand	BE (eV)
V_{Br}	n-type	CH_3COO^-	−4.36
Pb_i	n-type	CH_3COO^-	−2.03
Br_{Pb}	p-type	$CH_3NH_3^+$	−4.07

[a]Three relevant defects are listed along with their type, the ligand which passivates them, and the binding energy of the ligand at the defect site.

https://doi.org/10.1021/acs.jpclett.1c01243
J. Phys. Chem. Lett. 2021, 12, 6299–6304

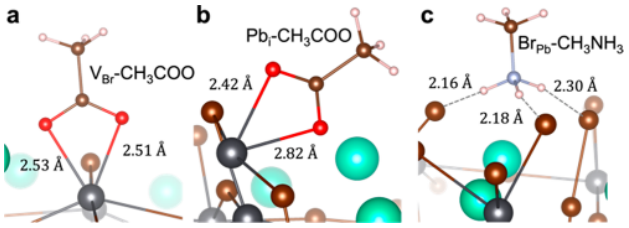

Figure 4. Local structure of the ligand passivated defects. (a) V_{Br} terminated by CH_3COO^-, (b) Pb_i terminated by CH_3COO^-, and (c) Br_{Pb} terminated by $CH_3NH_3^+$. In each panel, relevant interatomic distances are given in angstroms (Å).

nated Pb.[38] Meanwhile, methylammonium forms several H-bonds with the dangling surface Br, which we also observed for other *p*-type defects such as V_{Cs} (Supporting Information Figure S4).

Similar to unpassivated defects, we consider the formation energy of charged defects upon ligand passivation. We found that, even in the presence of charge, the formation energies of ligand-passivated defects are consistently much lower than the ones without passivation (by 3−5 eV, as shown in Figure S5), indicating greatly enhanced stability by passivation. Meanwhile, the charge transition levels reveal how the positioning of trap states, due to the defects, have been improved by the presence of the ligand, as shown in Figure 5a. Before passivation or termination ("no termination") surface defects generate deep trap states, but after passivation or termination ("terminated") these states are pushed toward the band edges or entirely eliminated from the bandgap altogether. For example before termination Pb_i has a transition level $E_{1|2}$ in the middle gap (~1.14 eV) which is removed after termination by acetate. Likewise Br_{Pb} possesses deep $E_{-2|-1}$ and $E_{-3|-2}$ transitions that are replaced by a shallow (energy closer to band edge) $E_{-2|0}$ transition. Meanwhile, for V_{Br}, the transition level $E_{0|1}$, just below the conduction band, moves very far from the conduction band edge.

The mechanism by which ligands yield dramatic changes to the transition levels in Figure 5a is demonstrated in Figure 5b−g. Parts b−d of Figure 5 show the highest occupied molecular orbital (HOMO) or lowest unoccupied molecular orbital (LUMO) of the n-type or p-type defects. These orbitals are highly localized, as expected for deep trap states. The deep traps can be removed or altered into shallow traps by a simple charge transfer process from the surface to the ligand (case of an n-type defect as in Figure 5e,f) or from the ligand to the surface (case of a p-type defect as in Figure 5g). Ultimately, this charge transfer process is responsible for the removal of these deep trap states and would indicate more balanced charge collection as observed experimentally after ligand passivation.[16]

It is anticipated that the removal of deep trap states in the bandgap due to surface defects by ligand passivation will lead to higher PLQY, as removing deep trap states should weaken Shockley−Read−Hall (SRH) nonradiative recombination of photoexcited electrons and holes.[39] To this end, it would be interesting to compute radiative[40] and nonradiative rates[41] that can provide further insight into experimentally measured PLQY and excited lifetimes. For example, recently SRH electron−hole recombination centers were investigated in $MAPbI_3$ using ab initio molecular dynamics.[42] It will also be important to consider excitonic effects[43] and exciton−phonon couplings. Other interesting pathways include investigation of the atomic composition of magic-sized clusters,[5,8] carrier conduction between surfaces and attached ligands,[44] or exploration into different ligand types.[17]

In summary, we have carefully investigated the structural and energetic properties of intrinsic charged defects at the surface of a prototypical LHP, $CsPbBr_3$, and their interplay with passivating ligands. Our work demonstrates that interstitials and antisites can have lower formation energy when they form at the surface due to stronger bond formation. Analysis of their charge transition levels shows two defects, Pb_i and Br_{Pb}, that simultaneously possess low formation energy and deep trap states due to dangling bonds and antibonding states, respectively. These deep trap states may be responsible for affecting optical properties such as photoluminescence. In addition, we explicitly explored the mechanism of defect passivation by molecular ligands wherein we established that ligands can effectively passivate not only vacancies but also interstitial atoms and antisites due to a charge transfer between the ligand and localized states of the defect. This work has

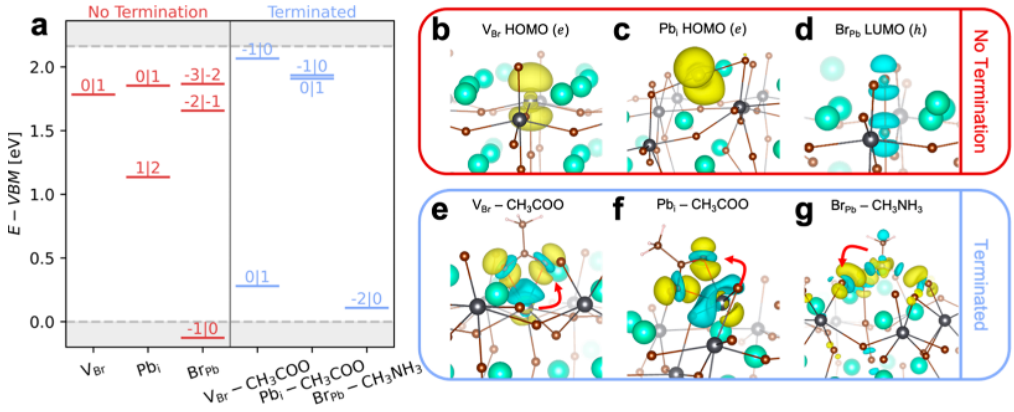

Figure 5. Explicit termination of charged defects by ligands on the surface of $CsPbBr_3$. (a) Charge transition levels of defects at $CsPbBr_3$ surface before and after ligand termination. Deep states are pushed shallower or ultimately removed after ligand passivation. (b−d) HOMO/LUMO of n-type/p-type defects at the surface of $CsPbBr_3$. The yellow/blue cloud is the charge of the localized electron/hole due to the defect which leads to trapping. (e−g) Charge transfer after ligand passivation, where the red arrow indicates the net direction of charge transfer. The yellow/blue cloud indicates an increase/decrease in the local charge density due to passivation.

https://doi.org/10.1021/acs.jpclett.1c01243
J. Phys. Chem. Lett. 2021, 12, 6299−6304

important implications in the field of LHPs, especially LHP devices where interfacial chemistry plays an important role in the optoelectronic properties and stability.

■ ASSOCIATED CONTENT

Supporting Information

The Supporting Information is available free of charge at https://pubs.acs.org/doi/10.1021/acs.jpclett.1c01243.

Further results and discussions regarding first-principles methodology, chemical potential energies, charged defect formation energies, comparison of defect formation at bulk and surface, computing ligand binding energies, ligand binding at VCs, and charged defect formation energies with ligands (PDF)

■ AUTHOR INFORMATION

Corresponding Authors

Jin Z. Zhang − *Department of Chemistry and Biochemistry, University of California, Santa Cruz, California 95064, United States;* orcid.org/0000-0003-3437-912X; Email: zhang@ucsc.edu

Tadashi Ogitsu − *Quantum Simulations Group, Lawrence Livermore National Laboratory, Livermore, California 94551, United States*; Email: ogitsu1@llnl.gov

Yuan Ping − *Department of Chemistry and Biochemistry, University of California, Santa Cruz, California 95064, United States;* orcid.org/0000-0002-0123-3389; Email: yuanping@ucsc.edu

Authors

Tyler J. Smart − *Department of Physics, University of California, Santa Cruz, California 95064, United States; Quantum Simulations Group, Lawrence Livermore National Laboratory, Livermore, California 94551, United States*

Hiroyuki Takenaka − *Department of Chemistry and Biochemistry, University of California, Santa Cruz, California 95064, United States*

Tuan Anh Pham − *Quantum Simulations Group, Lawrence Livermore National Laboratory, Livermore, California 94551, United States;* orcid.org/0000-0003-0025-7263

Liang Z. Tan − *The Molecular Foundry, Lawrence Berkeley National Laboratory, Berkeley, California 94720, United States;* orcid.org/0000-0003-4724-6369

Complete contact information is available at: https://pubs.acs.org/10.1021/acs.jpclett.1c01243

Notes

The authors declare no competing financial interest.

■ ACKNOWLEDGMENTS

This work is supported by the National Science Foundation under Grant No. CHE-1904547. Part of this work was performed under the auspices of the U.S. Department of Energy by Lawrence Livermore National Laboratory under Contract DE-AC52-07NA27344. T.O. is supported by the Computational Materials Sciences Program funded by the US Department of Energy, Office of Science, Basic Energy Sciences, Materials Sciences and Engineering Division. T.J.S. acknowledges the LLNL Graduate Research Scholar Program and funding support from LLNL LDRD 20-SI-004. T.A.P. acknowledges support from LLNL LDRD 20-SI-004. L.Z.T. was supported by the Molecular Foundry, a DOE Office of Science User Facility supported by the Office of Science of the U.S. Department of Energy under Contract No. DE-AC02-05CH11231. This research used resources of the Scientific Data and Computing center, a component of the Computational Science Initiative, at Brookhaven National Laboratory under Contract No. DE-SC0012704, the lux supercomputer at UC Santa Cruz, funded by NSF MRI Grant AST 1828315, the National Energy Research Scientific Computing Center (NERSC), a U.S. Department of Energy Office of Science User Facility operated under Contract No. DE-AC02-05CH11231, and the Extreme Science and Engineering Discovery Environment (XSEDE), which is supported by National Science Foundation Grant No. ACI-1548562.[45]

■ REFERENCES

(1) Jeong, M.; Choi, I. W.; Go, E. M.; Cho, Y.; Kim, M.; Lee, B.; Jeong, S.; Jo, Y.; Choi, H. W.; Lee, J.; et al. Stable perovskite solar cells with efficiency exceeding 24.8% and 0.3-V voltage loss. *Science* **2020**, *369*, 1615−1620.

(2) Kim, J. Y.; Lee, J. W.; Jung, H. S.; Shin, H.; Park, N. G. High-Efficiency Perovskite Solar Cells. *Chem. Rev.* **2020**, *120*, 7867−7918.

(3) Shi, J. J.; Li, Y. M.; Li, Y. S.; Li, D. M.; Luo, Y. H.; Wu, H. J.; Meng, Q. B. From Ultrafast to Ultraslow: Charge-Carrier Dynamics of Perovskite Solar Cells. *Joule* **2018**, *2*, 879−901.

(4) Kovalenko, M. V.; Protesescu, L.; Bodnarchuk, M. I. Properties and potential optoelectronic applications of lead halide perovskite nanocrystals. *Science* **2017**, *358*, 745−750.

(5) Vickers, E. T.; Chen, Z. Y.; Cherrette, V.; Smart, T.; Zhang, P.; Ping, Y.; Zhang, J. Z. Interplay between Perovskite Magic-Sized Clusters and Amino Lead Halide Molecular Clusters. *Research* **2021**, *2021*, 1.

(6) Wheeler, L. M.; Sanehira, E. M.; Marshall, A. R.; Schulz, P.; Suri, M.; Anderson, N. C.; Christians, J. A.; Nordlund, D.; Sokaras, D.; Kroll, T.; et al. Targeted Ligand-Exchange Chemistry on Cesium Lead Halide Perovskite Quantum Dots for High-Efficiency Photovoltaics. *J. Am. Chem. Soc.* **2018**, *140*, 10504−10513.

(7) De Roo, J.; Ibanez, M.; Geiregat, P.; Nedelcu, G.; Walravens, W.; Maes, J.; Martins, J. C.; Van Driessche, I.; Kovalenko, M. V.; Hens, Z. Highly Dynamic Ligand Binding and Light Absorption Coefficient of Cesium Lead Bromide Perovskite Nanocrystals. *ACS Nano* **2016**, *10*, 2071−2081.

(8) Liu, L.; Xu, K.; Vickers, E. T.; Allen, A.; Li, X. M.; Peng, L. J.; Zhang, J. Z. Varying the Concentration of Organic Acid and Amine Ligands Allows Tuning between Quantum Dots and Magic-Sized Clusters of $CH_3NH_3PbBr_3$ Perovskite: Implications for Photonics and Energy Conversion. *ACS Applied Nano Mater.* **2020**, *3*, 12379−12387.

(9) Vickers, E. T.; Enlow, E. E.; Delmas, W. G.; DiBenedetto, A. C.; Chowdhury, A. H.; Bahrami, B.; Dreskin, B. W.; Graham, T. A.; Hernandez, I. N.; Carter, S. A.; et al. Enhancing Charge Carrier Delocalization in Perovskite Quantum Dot Solids with Energetically Aligned Conjugated Capping Ligands. *ACS Energy Lett.* **2020**, *5*, 817−825.

(10) Ping, Y.; Zhang, J. Z. Spin-optotronic Properties of Organometal Halide Perovskites. *J. Phys. Chem. Lett.* **2018**, *9*, 6103−6111.

(11) Kim, Y.-H.; Zhai, Y.; Lu, H.; Pan, X.; Xiao, C.; Gaulding, E. A.; Harvey, S. P.; Berry, J. J.; Vardeny, Z. V.; Luther, J. M.; Beard, M. C. Chiral-induced spin selectivity enables a room-temperature spin light-emitting diode. *Science* **2021**, *371*, 1129−1133.

(12) Xue, J. J.; Wang, R.; Yang, Y. The surface of halide perovskites from nano to bulk. *Nat. Rev. Mater.* **2020**, *5*, 809−827.

(13) Zhang, J. Z. A "Cocktail" Approach to Effective Surface Passivation of Multiple Surface Defects of Metal Halide Perovskites Using a Combination of Ligands. *J. Phys. Chem. Lett.* **2019**, *10*, 5055−5063.

(14) Meggiolaro, D.; Mosconi, E.; De Angelis, F. Formation of Surface Defects Dominates Ion Migration in Lead-Halide Perovskites. *ACS Energy Lett.* **2019**, *4*, 779−785.

(15) Kang, J.; Wang, L. W. High Defect Tolerance in Lead Halide Perovskite $CsPbBr_3$. *J. Phys. Chem. Lett.* **2017**, *8*, 489−493.
(16) Wang, R.; Xue, J. J.; Wang, K. L.; Wang, Z. K.; Luo, Y. Q.; Fenning, D.; Xu, G. W.; Nuryyeva, S.; Huang, T. Y.; Zhao, Y. P.; et al. Constructive molecular configurations for surface-defect passivation of perovskite photovoltaics. *Science* **2019**, *366*, 1509−1513.
(17) Nenon, D. P.; Pressler, K.; Kang, J.; Koscher, B. A.; Olshansky, J. H.; Osowiecki, W. T.; Koc, M. A.; Wang, L. W.; Alivisatos, A. P. Design Principles for Trap-Free $CsPbX_3$ Nanocrystals: Enumerating and Eliminating Surface Halide Vacancies with Softer Lewis Bases. *J. Am. Chem. Soc.* **2018**, *140*, 17760−17772.
(18) Ten Brinck, S.; Zaccaria, F.; Infante, I. Defects in Lead Halide Perovskite Nanocrystals: Analogies and (Many) Differences with the Bulk. *ACS Energy Letters* **2019**, *4*, 2739−2747.
(19) Uratani, H.; Yamashita, K. Charge Carrier Trapping at Surface Defects of Perovskite Solar Cell Absorbers: A First-Principles Study. *J. Phys. Chem. Lett.* **2017**, *8*, 742−746.
(20) Yang, J. N.; Song, Y.; Yao, J. S.; Wang, K. H.; Wang, J. J.; Zhu, B. S.; Yao, M. M.; Rahman, S. U.; Lan, Y. F.; Fan, F. J.; et al. Potassium Bromide Surface Passivation on $CsPbI_{3-x}Br_x$ Nanocrystals for Efficient and Stable Pure Red Perovskite Light-Emitting Diodes. *J. Am. Chem. Soc.* **2020**, *142*, 2956−2967.
(21) Hassan, Y.; Park, J. H.; Crawford, M. L.; Sadhanala, A.; Lee, J.; Sadighian, J. C.; Mosconi, E.; Shivanna, R.; Radicchi, E.; Jeong, M.; et al. Ligand-engineered bandgap stability in mixed-halide perovskite LEDs. *Nature* **2021**, *591*, 72−77.
(22) Tian, Y.; Zhou, C. K.; Worku, M.; Wang, X.; Ling, Y. C.; Gao, H. W.; Zhou, Y.; Miao, Y.; Guan, J. J.; Ma, B. W. Highly Efficient Spectrally Stable Red Perovskite Light-Emitting Diodes. *Adv. Mater.* **2018**, *30*, 1707093.
(23) Ke, Y.; Wang, N. N.; Kong, D. C.; Cao, Y.; He, Y. R.; Zhu, L.; Wang, Y. M.; Xue, C.; Peng, Q. M.; Gao, F.; et al. Defect Passivation for Red Perovskite Light-Emitting Diodes with Improved Brightness and Stability. *J. Phys. Chem. Lett.* **2019**, *10*, 380−385.
(24) Abdi-Jalebi, M.; Andaji-Garmaroudi, Z.; Cacovich, S.; Stavrakas, C.; Philippe, B.; Richter, J. M.; Alsari, M.; Booker, E. P.; Hutter, E. M.; Pearson, A. J.; et al. Maximizing and stabilizing luminescence from halide perovskites with potassium passivation. *Nature* **2018**, *555*, 497−501.
(25) Wu, T.; Li, J. N.; Zou, Y. T.; Xu, H.; Wen, K. C.; Wan, S. S.; Bai, S.; Song, T.; McLeod, J. A.; Duhm, S.; et al. High-Performance Perovskite Light-Emitting Diode with Enhanced Operational Stability Using Lithium Halide Passivation. *Angew. Chem., Int. Ed.* **2020**, *59*, 4099−4105.
(26) Buin, A.; Pietsch, P.; Xu, J. X.; Voznyy, O.; Ip, A. H.; Comin, R.; Sargent, E. H. Materials Processing Routes to Trap-Free Halide Perovskites. *Nano Lett.* **2014**, *14*, 6281−6286.
(27) Yoo, D.; Woo, J. Y.; Kim, Y.; Kim, S. W.; Wei, S. H.; Jeong, S.; Kim, Y. H. Origin of the Stability and Transition from Anionic to Cationic Surface Ligand Passivation of All-Inorganic Cesium Lead Halide Perovskite Nanocrystals. *J. Phys. Chem. Lett.* **2020**, *11*, 652−658.
(28) Giannozzi, P.; Baroni, S.; Bonini, N.; Calandra, M.; Car, R.; Cavazzoni, C.; Ceresoli, D.; Chiarotti, G. L.; Cococcioni, M.; Dabo, I.; et al. QUANTUM ESPRESSO: a modular and open-source software project for quantum simulations of materials. *J. Phys.: Condens. Matter* **2009**, *21*, 395502.
(29) Yang, R. X.; Tan, L. Z. Understanding size dependence of phase stability and band gap in $CsPbI_3$ perovskite nanocrystals. *J. Chem. Phys.* **2020**, *152*, 034702.
(30) Garrity, K. F.; Bennett, J. W.; Rabe, K. M.; Vanderbilt, D. Pseudopotentials for high-throughput DFT calculations. *Comput. Mater. Sci.* **2014**, *81*, 446−452.
(31) Meggiolaro, D.; De Angelis, F. First-Principles Modeling of Defects in Lead Halide Perovskites: Best Practices and Open Issues. *ACS Energy Lett.* **2018**, *3*, 2206−2222.
(32) van Setten, M. J.; Giantomassi, M.; Bousquet, E.; Verstraete, M. J.; Hamann, D. R.; Gonze, X.; Rignanese, G. M. The PSEUDODOJO: Training and grading a 85 element optimized norm-conserving pseudopotential table. *Comput. Phys. Commun.* **2018**, *226*, 39−54.
(33) Sundararaman, R.; Ping, Y. First-principles electrostatic potentials for reliable alignment at interfaces and defects. *J. Chem. Phys.* **2017**, *146*, 104109.
(34) Li, S.; Shi, Z. F.; Zhang, F.; Wang, L. T.; Ma, Z. Z.; Yang, D. W.; Yao, Z. Q.; Wu, D.; Xu, T. T.; Tian, Y. T.; et al. Sodium Doping-Enhanced Emission Efficiency and Stability of $CsPbBr_3$ Nanocrystals for White Light-Emitting Devices. *Chem. Mater.* **2019**, *31*, 3917−3928.
(35) Aragoni, M. C.; Arca, M.; Coles, S. L.; Devillanova, F. A.; Hursthouse, M. B.; Isaia, F.; Lippolis, V. Reactivity of phosphono-dithioato-dppt Ni-II mixed ligand complexes with halogens: First example of a metal-coordinating tribromide anion. *Dalton Trans.* **2012**, *41*, 6611−6613.
(36) Huang, H.; Bodnarchuk, M. I.; Kershaw, S. V.; Kovalenko, M. V.; Rogach, A. L. Lead Halide Perovskite Nanocrystals in the Research Spotlight: Stability and Defect Tolerance. *ACS Energy Lett.* **2017**, *2*, 2071−2083.
(37) Ravi, V. K.; Santra, P. K.; Joshi, N.; Chugh, J.; Singh, S. K.; Rensmo, H.; Ghosh, P.; Nag, A. Origin of the Substitution Mechanism for the Binding of Organic Ligands on the Surface of $CsPbBr_3$ Perovskite Nanocubes. *J. Phys. Chem. Lett.* **2017**, *8*, 4988−4994.
(38) Wu, Z. F.; Jiang, M. W.; Liu, Z. H.; Jamshaid, A.; Ono, L. K.; Qi, Y. B. Highly Efficient Perovskite Solar Cells Enabled by Multiple Ligand Passivation. *Adv. Energy Mater.* **2020**, *10*, 1903696.
(39) Zhang, X.; Shen, J. X.; Van de Walle, C. G. First-Principles Simulation of Carrier Recombination Mechanisms in Halide Perovskites. *Adv. Energy Mater.* **2020**, *10*, 1902830.
(40) Wu, F.; Rocca, D.; Ping, Y. Dimensionality and anisotropicity dependence of radiative recombination in nanostructured phosphorene. *J. Mater. Chem. C* **2019**, *7*, 12891−12897.
(41) Wu, F.; Smart, T. J.; Xu, J. Q.; Ping, Y. Carrier recombination mechanism at defects in wide band gap two-dimensional materials from first principles. *Phys. Rev. B: Condens. Matter Mater. Phys.* **2019**, *100*, 081407.
(42) Chu, W. B.; Zheng, Q. J.; Prezhdo, O. V.; Zhao, J.; Saidi, W. A. Low-frequency lattice phonons in halide perovskites explain high defect tolerance toward electron-hole recombination. *Sci. Adv.* **2020**, *6*, No. eaaw7453.
(43) Ping, Y.; Rocca, D.; Galli, G. Electronic excitations in light absorbers for photoelectrochemical energy conversion: First principles calculations based on many body perturbation theory. *Chem. Soc. Rev.* **2013**, *42*, 2437−2469.
(44) Brawand, N. P.; Goldey, M. B.; Voros, M.; Galli, G. Defect States and Charge Transport in Quantum Dot Solids. *Chem. Mater.* **2017**, *29*, 1255−1262.
(45) Towns, J.; Cockerill, T.; Dahan, M.; Foster, I.; Gaither, K.; Grimshaw, A.; Hazlewood, V.; Lathrop, S.; Lifka, D.; Peterson, G. D.; et al. XSEDE: Accelerating Scientific Discovery. *Comput. Sci. Eng.* **2014**, *16*, 62−74.

https://doi.org/10.1021/acs.jpclett.1c01243
J. Phys. Chem. Lett. 2021, 12, 6299−6304